Effective Vision- and SoC-Based Fall Detection for the Elderly

Kuo-Liang Chung[a], Chi-Huang Liao[b], Li-Ting Liu[a], De-Hao Liu[a], Yu-Sheng Chan[a], and Jen-Shun Cheng[a]

[a]Department of Computer Science and Information Engineering National Taiwan University of Science and Technology Keelung Road, Taipei, 10672, Taiwan, R.O.C.
[b]System Online Co. Ltd., 10F, No. 263, Section 3, Jhong-Siao East Rd., Taipei, 10654, R.O.C.

ABSTRACT

In this paper, we propose a novel Vision- and system on chip (SoC)- based fall detection method for the elderly. Once, a fall event is detected, an alarm signal is immediately sent out to query first aid to the elderly. Our novel fall detection method consists of five effective steps: checking whether the light condition has been stabilized, GMM-based background and foreground estimation, a new strategy to solve the foreground lag problem, solving the false fall detection problem when light comes from a neighboring room, as well as the fall detection determination and the general-purpose input/output based warning mechanism. Based on the test videos, the experiments have been carried out demonstrate that our proposed fall detection method can meet the real-time, low cost, and high accuracy demands.

Keywords: Fall detection, Health care, Vision, Real-time, System on chip (SoC)

1. INTRODUCTION

According to the report in [13], the percentage of the people aged 65 or older in the world will be 16% in 2050. The main reason is that the number of elderly people is increasing due to the growth of health care provided by hospitals and the medical advancements. Especially, if the elderly patient falls in the room. Once a fall event occurs for an older person, if a fall detection signal can be sent out in time to query first aid, the person can be rescued. The previous fall detection methods can be classified into the following four categories: the wearable device-based category [10], [3], the ambiance sensor-based category [11], [12], the RGB-D (red-green-blue color camera plus depth sensor) based category [1], [2], and the camera-based category [7], [8], [9].

The main weakness in the wearable device-based category is that it is inconvenient for the elderly to carry a wearable device all day in order to avoid falls. The main constraint of the wearable device-based fall detection category is that it is inconvenient for the elderly to carry a wearable device all day in order to avoid falls. The hardware cost of the camera and the bundled personal computer is also not cheap for the consumers. We take the two methods [8], [9] as the comparative methods because the two methods are camera-based approach which is similar to ours.

The above-mentioned weaknesses motivated us to propose a novel vision- and SoC-based fall detection method. Our proposed method can meet the real-time, low cost, and high accuracy demands. In addition, the comprehensive experiments have been carried out to demonstrate that in terms of commonly used metrics, accuracy, precision and recall, our proposed vision- and SoC-based fall detection method outperforms the state-of-the-art methods [8], [9].

2. THE HARDWARE SETTING

As depicted in Fig. 1(a), the two hardware facilities used in our method are the SoC 'Hisilicon-Hi3516CV300' with size 37mm × 37mm (see Fig. 1(b)) and the bundled camera 'M12-4IR(3MP)-C'; they are combined together and are arranged at location A. In Fig. 1(a), 'B' denotes the table, 'C' denotes the bed, and 'D' denotes the clothes chest in the room. The side-view of the room is depicted in Fig. 1(c).

Kuo-Liang: klchung01@gmail.com; phone +866 2 2737 6771; supported by MOST-107-2622-E-011-030-CC3.

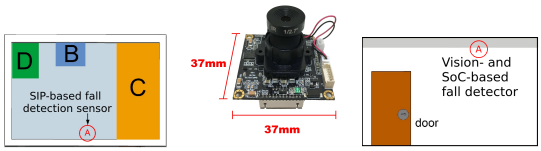

(a) (b) (c)

Figure 1. The depiction of our hardware setting in the room. (a) The top-view of the room. (b) The used SoC 'Hisilicon-Hi3516CV300'. (c) The side-view of the room to the door.

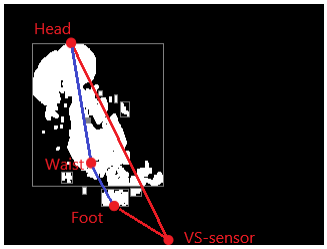

Figure 2. The depiction of the foreground distortion problem caused by the perspective projection from the foreground to camera.

3. THE PROPOSED FALL DETECTION METHOD

Because the camera is set up in a high position under the ceiling, as shown in Fig. 2, we observe that the perspective projection from the camera to the head H, waist W, and feet F of the foreground often leads to $\overline{HW} \gg \overline{WF}$, making the traditionally used gradient information unreliable. It motivated us to develop a new approach to solve the fall detection method under this environment. Our method is descriped as below.

3.1 Step 1: Checking Whether the Light Condition has been Stabilized or not

Let I_t and I_{t-1} denote the two images at time instances t and $t-1$, respectively. In order to test whether the light condition has been stabilized or not before starting the formal fall detection task, we first compute the absolute difference between the average gray value of I_t and that of I_{t-1}, and then we compute the absolute average difference which can be calculated quickly by the following building histogram computation-based way:

$$D_{avg} = |\frac{\sum_{i=0}^{255}(i \times H_t(i))}{320 \times 240} - \frac{\sum_{j=0}^{255}(j \times H_{t-1}(j))}{320 \times 240}| \quad (1)$$

where H_t and H_{t-1} denote the two histograms of I_t and I_{t-1}, respectively, in which each image is of size 320×240. The histogram of each image can be quickly calculated by calling the building function 'HI_MPI_IVE_Hist' in SoC.

Further, we check whether the value of D_{avg} is less than the specific threshold or not, and empirically the threshold is set to 100. If not, it means that the light condition has not been stabilized and we go to Step 1; otherwise, we go to Step 2.

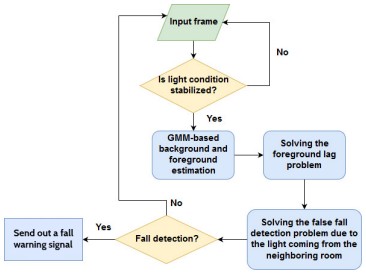

Figure 3. The flow of our new fall detection method.

Table 1. BUILDING FUNCTIONS IN SoC.

Subroutine Name	Functionality
HI_MPI_IVE_And	logical AND operation
HI_MPI_IVE_CCL	connected component labeling
HI_MPI_IVE_Dilate	dilate operation
HI_MPI_IVE_Erode	erosion operation
HI_MPI_IVE_GMM2	background estimation
HI_MPI_IVE_Hist	histogram calculation
HI_MPI_IVE_Or	logical OR operation
HI_MPI_IVE_Sobel	Sobel edge detector
HI_MPI_IVE_Sub	subtraction operation

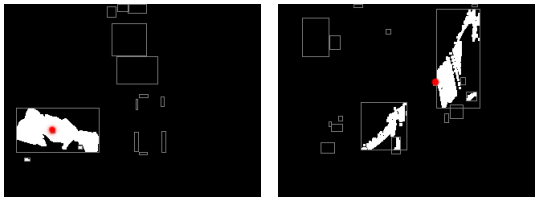

(a) (b)

Figure 4. One example for the false fall detection problem and its solution. (a) The foreground is approaching the door. (b) The false foreground caused by opening the door.

3.2 Step 2: GMM-based Background and Foreground Estimation

We first apply the GMM-based building function 'HI_MPI_IVE_GMM2' to estimate the background model, and then generate the foreground model by subtracting the estimated background from the current image frame. Secondly, we apply an erosion operation 'HI_MPI_IVE_Erode' to remove the small foreground component, and then a dilation operation 'HI_MPI_IVE_Dilate' is applied to connect the nearest neighboring foreground components to form a more complete foreground component. When the foreground stays in some place for a period of time, the foreground will gradually melt into the background, causing the foreground melting phenomenon.

3.3 Step 3: Efficient Strategy to Solve the Foreground Lag Problem

In the foreground melting period, if the foreground leaves one place to another place, it leads to two foregrounds, one in the old place and the other in the new place.

In our strategy, first, we apply the connected component labeling function 'HI_MPI_IVE_CCL' to label each foreground component. Let F_{old} and F_{new} denote the old foreground map residing in the background and the newly generated foreground map, respectively. In the two foreground maps, F_{old} and F_{new}, each white foreground pixel is denoted by '1', and each background pixel is denoted by '0'. After that, we perform the subtraction operation 'HI_MPI_IVE_Sub' on I_t and I_{t-1} to obtain the difference image D. Then, we calculate the absolute value of each resultant pixel-value in D. Based on the specified threshold T (empirically we set $T = 10$), the difference image D is further binarized and the binarized image D_b, in which each white pixel '1' often appears on the boundary of the current foreground. In other words, the binary image D_b does represent the boundary of the current foreground.

For each selected white pixel, we use it as the seed to obtain the corresponding connected component in F_{new} by calling the connected component labeling function 'HI_MPI_IVE_CCL'. As a result, all the connected components in F_{new} can be collected and they are denoted by the set C. We now calculate the centroid of C by

$$(x_c, y_c) = (\frac{m_{10}}{m_{00}}, \frac{m_{01}}{m_{00}}) \tag{2}$$

in which m_{10}, m_{01}, and m_{00} denote the traditional first-order, first-order, and zero-order moments of C.

The centroid in Eq. (2) is used to identify the center of the true foreground.

3.4 Step 4: Solving the False Fall Detection Problem

When the foreground is opening the door, as shown in Fig. 4(a), at that moment, the light coming from the neighboring room into the current room usually makes the centroid of the newly generated foreground go back to the current room. As shown in Fig. 4(b), the red circle denotes the centroid of the newly generated foreground back to the current room. In Fig. 4(a), the red circle denotes the centroid of the new foreground generated by the light coming from the neighboring room.

Considering three consecutive images, I_{t-2}, I_{t-1}, and I_t, we perform the Sobel edge detection 'HI_MPI_IVE_Sobel' on the three images to obtain the three edge maps, E_{t-2}, E_{t-1}, and E_t. Next, we perform the difference operation between two consecutive edge maps, and obtain the two boundary maps $B_{t-1} = E_{t-1} - E_{t-2}$ and $B_t = E_t - E_{t-1}$. Further, we perform the logical AND operation 'HI_MPI_IVE_And ' on B_{t-1} and B_t, and we have $B'_t = B_{t-1} \cap B_t$. Let the number of white pixels in B'_t be $|B'_t|$. In order to enhance the fall detection robustness, we perform $B'_t = B'_t \cup B'_{t-1} \cup B'_{t-2} \cup B'_{t-3} \cup B'_{t-4}$ to avoid the light change effect on the foreground estimation because of the light coming from the neighboring room. Then, we calculate the centroid of B'_t, (x'_c, y'_c). If (x'_c, y'_c) resides in the special door area, marked in advance, we claim that the foreground has left the current room, and we ignore whatever the centroid value has been calculated; otherwise, it means that the centroid (x_c, y_c) of the foreground is still located in the current room, and we claim that the foreground is still in the current room.

3.5 Step 5: Fall Detection Determination

If the centroid of the detected foreground is on the floor area, then the detected foreground is considered to be in the current room. In addition, if the centroid stays in a fixed location for more than t seconds, e.g. t = 10, a fall detection alarm signal is sent out; otherwise, go to Step 1.

4. EXPERIMENTAL RESULTS

The thorough experimentation has been carried out to demonstrate the detection accuracy merit of our vision- and SoC-based fall detection method when compared with the two image processing- and PC (personal computer)-based fall detection methods [8], [9].

First, four parameters, true positive (TP), true negative (TN), false positive (FP), and false negative (FN), are defined by
TP: the number of fall events correctly detected by the concerned method.
TN: the number of non-fall events correctly detected by the concerned method.
FP: the number of non-fall events incorrectly detected as fall events by the concerned method.
FN: the number of fall events incorrectly detected as non-fall events by the concerned method.

The performance evaluation metrics, accuracy, precision, recall, and error-rate, are defined by

$$Accuracy\ (Ac) = \frac{TP + TN}{TP + FP + TN + FN};\ Precision(Pr) = \frac{TP}{TP + FP} \tag{3}$$

$$Recall\ (Rc) = \frac{TP}{TP + FN};\ Error\text{-}rate\ (Er) = 1 - Accuracy \tag{4}$$

where 'Accuracy' denotes the total successful fall and non-fall detection rate of all events; 'Precision' denotes the successful fall detection rate of all fall events; 'Recall' denotes the successful rate of all fall reports; 'Error-rate' is equal to '1 - Accuracy'.

In the fall event simulation, five types are considered in the experiment, namely backward, forward, lateral left, lateral right, and syncope fall types. In the non-fall event simulation, the postures include walking, sitting, standing, and crouching. Each posture is simulated five times, so there are five videos for each posture. Totally, we have 45 videos covering the nine postures. Table 2 tabulates the performance comparison among our method and the two concerned methods. In Table 2, we observe that our method has 95.6% detection accuracy, 4.4% (= 1 - 95.6%) error-rate, 96% detection precision, and 96% detection recall. In summary, our method has the best accuracy and the least error-rate.

Table 2. ACCURACY COMPARISON AMONG THE CONCERNED METHODS.

	TP	TN	FP	FN	Ac(%)	Pr(%)	Re(%)	Er(%)
Proposed	24	19	1	1	**95.6**	96	**96**	**4.4**
Nguyen *et al.* [9]	11	20	0	14	68.9	100	44	31.1
Lin *et al.* [8]	20	14	6	5	75.6	76.9	80	24.4

5. CONCLUSION

We have presented our Vision- and SoC-based fall detection method for the elderly. Our method consists of five steps, and among them, in particular, we propose new strategies to solve two practical and challenging problems, the foreground lag problem and the false fall detection problem when opening the door. The thorough experimental data have demonstrated that our method can meet the low-cost, low-power, high accuracy, and real-time healthcare demands.

References

[1] A. Abobakr, M. Hossny, and S. Nahavandi, "A Skeleton-Free Fall Detection System From Depth Images Using Random Decision Forest," *IEEE Systems Journal,* pp. 1-12, Dec. 2017.

[2] Z. P. Bian, J. Hou, L. P. Chau, and N. M. Thalmann, "Fall Detection Based on Body Part Tracking Using a Depth Camera," *IEEE Journal of Biomedical and Health Informatics,* vol. 19, no. 2, pp. 430-439, Mar. 2015.

[3] M. Cheffena, "Fall Detection Using Smartphone Audio Features," *IEEE Journal of Biomedical and Health Informatics,* vol. 20, no. 4, pp. 1073-1080, Jul. 2016.

[4] B. Erol, M. G. Amin, and B. Boashash "Range-Doppler Radar Sensor Fusion for Fall Detection," *2017 IEEE, Radar Conference (RadarConf),* pp. 0819 - 0824, May. 2017.

[5] L. J. Kau and C. S. Chen, "A Smart Phone-Based Pocket Fall Accident Detection, Positioning, and Rescue System," *IEEE Journal of Biomedical and Health Informatics ,* vol. 19, no. 1, pp. 44-56, jan. 2015.

[6] X. Kong, L. Meng, and H. Tomiyama, "Fall Detection for Elderly Persons Using a Depth Camera," *Advanced Mechatronic Systems (ICAMechS), 2017 International Conference on,* pp. 269-273, Dec. 2017.

[7] Y. T. Liao, C. L. Huang, S. C. Hsu, "Slip and Fall Event Detection Using Bayesian Belief Network," *Pattern Recognition,* vol. 45, no. 1, pp. 24-32, Jan. 2012.

[8] C. Y. Lin, S. M. Wang, J. W. Hong, L.W Kang, and C. L. Huang, "Vision-Based Fall Detection through Shape Features," *Multimedia Big Data (BigMM), 2016 IEEE Second International Conference on,* pp. 237-240, Apr. 2016.

[9] V. D. Nguyen, M. T. Le, A. D. Do, H. H. Duong, T. D. Thai, and D. H. Tran "An Efficient Camera-based Surveillance for Fall Detection of Elderly People," *Industrial Electronics and Applications (ICIEA), 2014 IEEE 9th Conference on,* pp. 994-997, Jun. 2014.

[10] P. Pierleoni, A. Belli, L. Palma, M. Pellegrini, L. Pernini, and S. Valenti, "A High Reliability Wearable Device for Elderly Fall Detection," *IEEE Sensors Journal,* vol. 15, no. 8, pp. 4544-4553, Aug. 2015.

[11] K. Shiba, T. Kaburagi, and Y. Kurihara, "Fall Detection Utilizing Frequency Distribution Trajectory by Microwave Doppler Sensor," *IEEE Sensors Journal,* vol. 17, no. 22, pp. 7561-7568, Nov. 2017.

[12] B. Y. Su, K. C. Ho, M. J. Rantz, and M. Skubic, "Doppler Radar Fallactivity Detection Using the Wavelet Transform," *IEEE Transactions on Biomedical Engineering,* vol. 62, no. 3, pp. 865–875, Mar. 2015.

[13] United Nations, World Population Prospects: The 2008 Revision-Comprehensive Tables: UN, 2010.